

Quantum anomalous Hall effect in twisted bilayer graphene

Wen-Xiao Wang(王文晓), Yi-Wen Liu(刘亦文), and Lin He(何林)

Citation: Chin. Phys. B, 2025, 34 (**4**): 047301. DOI: 10.1088/1674-1056/adb38a
Journal homepage: http://cpb.iphy.ac.cn; http://iopscience.iop.org/cpb

What follows is a list of articles you may be interested in

Moiré physics in two-dimensional materials: Novel quantum phases and electronic properties

Zi-Yi Tian(田子弈), Si-Yu Li(李思宇), Hai-Tao Zhou(周海涛), Yu-Hang Jiang(姜宇航), and Jin-Hai Mao(毛金海)
Chin. Phys. B, 2025, 34 (**2**): 027301. DOI: 10.1088/1674-1056/ad9e96

Strain-modulated antiferromagnetic Chern insulator in $NiOsCl_6$ monolayer

Bin Wu(武斌), Na Li(李娜), Xin-Lian Chen(陈新莲), Wei-Xiao Ji(纪维霄), Pei-Ji Wang(王培吉), Shu-Feng Zhang(张树峰), and Chang-Wen Zhang(张昌文)
Chin. Phys. B, 2024, 33 (**12**): 127301. DOI: 10.1088/1674-1056/ad84cb

Intrinsic valley-polarized quantum anomalous Hall effect in a two-dimensional germanene/MnI_2 van der Waals heterostructure

Xiao-Jing Dong(董晓晶) and Chang-Wen Zhang(张昌文)
Chin. Phys. B, 2024, 33 (**7**): 077303. DOI: 10.1088/1674-1056/ad4bbd

Recent progress on valley polarization and valley-polarized topological states in two-dimensional materials

Fei Wang(王斐), Yaling Zhang(张亚玲), Wenjia Yang(杨文佳), Huisheng Zhang(张会生), and Xiaohong Xu(许小红)
Chin. Phys. B, 2024, 33 (**1**): 017306. DOI: 10.1088/1674-1056/ad0713

Low-damage photolithography for magnetically doped $(Bi,Sb)_2Te_3$ quantum anomalous Hall thin films

Zhiting Gao(高志廷), Minghua Guo(郭明华), Zichen Lian(连梓臣), Yaoxin Li(李耀鑫), Yunhe Bai(白云鹤), Xiao Feng(冯硝), Ke He(何珂), Yayu Wang(王亚愚), Chang Liu(刘畅), and Jinsong Zhang(张金松)
Chin. Phys. B, 2023, 32 (**11**): 117303. DOI: 10.1088/1674-1056/ad0147

TOPICAL REVIEW — Moiré physics in two-dimensional materials

Quantum anomalous Hall effect in twisted bilayer graphene

Wen-Xiao Wang(王文晓)[1,5], Yi-Wen Liu(刘亦文)[2], and Lin He(何林)[3,4,†]

[1] *Hebei Advanced Thin Films Laboratory, Hebei Normal University, Shijiazhuang* 050024, *China*
[2] *Department of Condensed Matter Physics, Weizmann Institute of Science, Rehovot* 7610001, *Israel*
[3] *Center for Advanced Quantum Studies, Department of Physics, Beijing Normal University, Beijing* 100875, *China*
[4] *Key Laboratory of Multiscale Spin Physics, Ministry of Education, Beijing* 100875, *China*
[5] *Postdoctoral Research Station at Hebei Normal University, Shijiazhuang* 050024, *China*

(Received 12 October 2024; revised manuscript received 7 December 2024; accepted manuscript online 7 February 2025)

Recent advancements in two-dimensional van der Waals moiré materials have unveiled the captivating landscape of moiré physics. In twisted bilayer graphene (TBG) at 'magic angles', strong electronic correlations give rise to a diverse array of exotic physical phenomena, including correlated insulating states, superconductivity, magnetism, topological phases, and the quantum anomalous Hall (QAH) effect. Notably, the QAH effect demonstrates substantial promise for applications in electronic and quantum computing devices with low power consumption. This article focuses on the latest developments surrounding the QAH effect in magic-angle TBG. It provides a comprehensive analysis of magnetism and topology — two crucial factors in engineering the QAH effect within magic-angle TBG. Additionally, it offers a detailed overview of the experimental realization of the QAH effect in moiré superlattices. Furthermore, this review highlights the underlying mechanisms driving these exotic phases in moiré materials, contributing to a deeper understanding of strongly interacting quantum systems and facilitating the manipulation of new material properties to achieve novel quantum states.

Keywords: quantum anomalous Hall effect, magic-angle twisted bilayer graphene, moiré superlattices

PACS: 73.22.Pr, 73.21.Cd, 73.20.–r

DOI: 10.1088/1674-1056/adb38a **CSTR:** 32038.14.CPB.adb38a

1. Introduction

Van der Waals moiré materials, engineered through lattice mismatch in heterostructures or rotational angles in homostructures of two-dimensional (2D) materials such as graphene, transition metal dichalcogenides (TMDs), and hexagonal boron nitride (h-BN), have attracted remarkable attention in recent years. The wavelength of moiré superlattices can be precisely controlled by selecting suitable 2D materials with distinct lattice constants or by adjusting the twist angles. These moiré superlattices introduce an additional degree of freedom to modulate the properties of 2D materials. Notably, superlattices with long-wavelength periodicities often give rise to flat bands at low energy, providing a platform for the emergence of strong electron–electron interactions and a variety of exotic quantum phenomena. These phenomena include correlated insulating states, ferromagnetic states, Chern insulator states, and superconductivity.[1–5]

Recently, a novel quantum phenomenon in van der Waals superlattices, known as the quantum anomalous Hall (QAH) effect, has been observed.[6–9] The QAH effect is characterized by topologically invariant chiral edge states without dissipation, as illustrated in Fig. 1(a). These states offer immense potential for low-dissipation electronic devices and quantum computing applications. As a result, the QAH effect has become a focal point of research in quantum Hall physics. This phenomenon was first experimentally realized in magnetically doped topological insulators (TIs).[6] Three-dimensional TIs exhibit gapless helical surface states with a Dirac-like dispersion protected by time-reversal symmetry (TRS), as illustrated in Fig. 1(b). Magnetic doping breaks TRS, inducing a gap in TI films and transforming them into QAH systems with chiral edge states. The QAH effect has been observed in magnetically doped TIs at extremely low temperatures, typically hundreds of milli-Kelvin.[6,10] Compared to the individual Cr or V doping,[6,11–13] magnetic modulation doping and codoping Cr and V elements in topological insulators were developed to increase the temperature of QAH effect to about 1–1.5 K.[14,15] An alternative approach to achieving the QAH effect was also proposed, which involves utilizing intrinsic magnetic TIs such as $MnBi_2Te_4$. The $C = 1$ QAH effect was realized in $MnBi_2Te_4$ at 1.4 K.[7] Additionally, the heterostructures formed by $MnBi_2Te_4$ with Bi_2Te_3 or Sb_2Te_3 not only possess robust magnetic order, but also have the potential to increase the quantization temperature.[16–18] For example, a $MnBi_2Te_4$–$[Sb_2Te_3]_{5QL}$–$MnBi_2Te_4$ heterostructure was predicted to increase the magnetic transition temperature to 42 K.[18] Above all, achieving full quantization of the QAH effect at higher critical temperatures remains a significant chal-

†Corresponding author. E-mail: helin@bnu.edu.cn

© 2025 Chinese Physical Society and IOP Publishing Ltd. All rights, including for text and data mining, AI training, and similar technologies, are reserved.

lenge, motivating intense investigations into new systems.

Previous investigations of the QAH effect in TIs have emphasized the essential role of spin–orbit coupling (SOC), without considering the impact of electronic correlations. These correlations have the potential to induce unconventional quantum phenomena, such as the QAH and fractional quantum anomalous Hall (FQAH) phases.[19,20] Theoretical studies predicted that introducing flat bands in magnetic TIs could foster electron correlations, potentially realizing the FQAH effect.[10] The emergence of moiré materials has established electronic interactions as a promising avenue for realizing these quantum phenomena. As illustrated in Fig. 1(c), long-period moiré superlattices exhibit relatively flat bands. When the kinetic energy determined by the bandwidth is smaller than the Coulomb interaction energy, electron–electron interactions become pronounced, leading to a variety of correlated phases, such as correlated insulators and superconductivity. In particular, strong interactions between electrons can give rise to orbital magnetism and topological properties, both of which are favorable to achieving QAH and FQAH effects. Among moiré materials, magic-angle twisted bilayer graphene (TBG) stands out as an ideal system for exploring these exotic quantum behaviors and has garnered extensive research. In this article, we review recent advance in the QAH effect in TBG, both theoretically and experimentally. Initially, the single-particle band structure of TBG, tuned by twist angles, is briefly introduced. In the presence of strong correlations, the predicted orbital magnetism and topologically nontrivial phases in magic-angle TBG are discussed in Section 3. Subsequently, Sections 4–6 detail the experimental realization of the anomalous Hall (AH), QAH, and FQAH effects, respectively, and explore the underlying mechanisms. Additionally, we summarize various other 2D systems related to the QAH effect. Finally, we discuss the challenges and future direction of this dynamic and promising field of research.

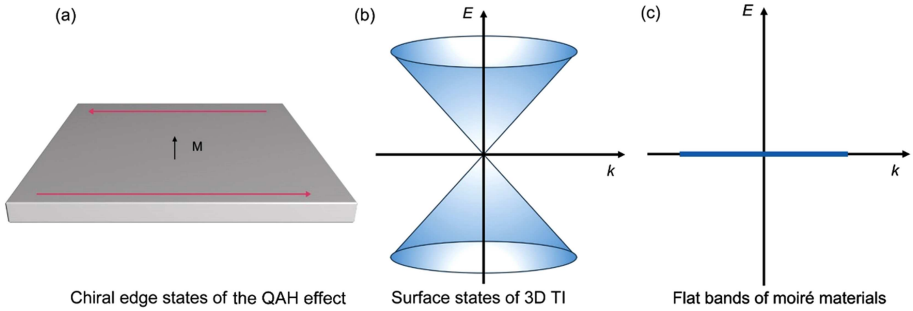


Fig. 1. QAH effect, characterized by the opening of an exchange gap, in both magnetic TIs and moiré superlattice systems. (a) QAH effect with chiral edge states. (b) Surface states of three-dimensional TIs. (c) Flat band structure of moiré materials.

2. Band structure of twisted bilayer graphene

Single-layer graphene, with its honeycomb lattice structure, is characterized by a linear Dirac cone at low energies. This feature endows graphene with numerous distinctive properties, such as high carrier mobility, a non-zero Berry's phase, and a vanishing mass of Dirac fermions near the charge neutrality point. Consequently, the integer and fractional quantum Hall effects have been observed in single-layer graphene systems.[21,22] In 2005, Kane *et al.* predicted the possibility of realizing the quantum spin Hall effect in single-layer graphene by introducing SOC.[23] These results suggest that graphene is an ideal system for realizing quantum Hall-related states.[23–25]

When two graphene sheets are overlaid at certain twist angles, they form TBG with periodic moiré patterns. The atomic registry of moiré patterns in TBG ranges from AA, AB, to BA stacking orders, as shown in Figs. 2(a) and 2(b).[1] In reciprocal space, the intersection of the two Dirac cones results in the formation of Van Hove singularities (VHSs) flanking the Dirac point due to significant interlayer interactions, as shown in Figs. 2(c) and 2(e).[26–29] The energy difference between the two VHSs is described by the equation $\Delta E_{\mathrm{VHS}} \approx \hbar v_{\mathrm{F}} \Delta K - 2t_\theta$, where $\Delta K = 2|\boldsymbol{K}| \sin\theta/2$ is the relative shift of the two Dirac points in momentum space, v_{F} is the Fermi velocity, t_θ represents the interlayer coupling, and $\hbar$ is the reduced Planck constant. This equation reveals a strong correlation between ΔE_{VHS} and both t_θ and the twist angle θ. Experimental evidence has established a robust link between t_θ and interlayer spacing. Furthermore, it has been observed that ΔE_{VHS} undergoes large oscillations due to variations in the interlayer coupling at a constant twist angle.[30] Notably, ΔE_{VHS} decreases as the twist angle θ decreases, as clearly demonstrated by scanning tunneling microscopy measurements.[26,31,32]

Specifically, when the twist angle is sufficiently small, a series of twist angles called "magic angles" emerge, such as 1.05°, 0.5°, 0.35°, 0.24° and 0.2°.[33] The single-particle band structure of TBG at these magic angles predicts the emergence of flat bands with nearly no dispersion near the Fermi level, as shown in Fig. 2(d). The small dispersion signifies that the effective mass of the electrons is substantially large, resulting in a small kinetic energy. The band width of flat bands represents the kinetic energy, denoted by W. The strength of Coulomb interactions can be expressed by the formula $U = e^2/(4\pi\varepsilon_0\varepsilon_{\mathrm{r}}L)$,

where ε_0 and ε_r are the dielectric constants, e is the electron charge, and L is the superlattice periodicity of TBG. When W is smaller than U, the Coulomb interactions dominate the electronic properties of TBG. The intensity of electronic interactions is influenced by factors such as the bandwidth of the flat bands, the energy gap between the two flat bands, and the gap between the flat bands and the higher dispersive bands above them.[34–41] These factors are shaped by various sample-specific details, such as the precise twist angle, stacking configuration and strain.[5,42–44] Notably, the energy gap between the two flat bands and the higher dispersive bands is significantly affected by lattice relaxation. The relaxation process is driven by the competition between van der Waals interaction energy and the elastic energy of TBG. The resulting lattice reconstruction plays an important role in creating an energy gap that isolates the flat bands from the higher energy bands, thereby facilitating the onset of electronic interactions.[44–49] Within the realm of electronic interactions, a multitude of correlated states have been realized, such as correlated insulating states, superconductivity, magnetism, and topological phases. The strong electronic interactions in these twisted systems open a novel avenue for the realization of exotic quantum phenomena.

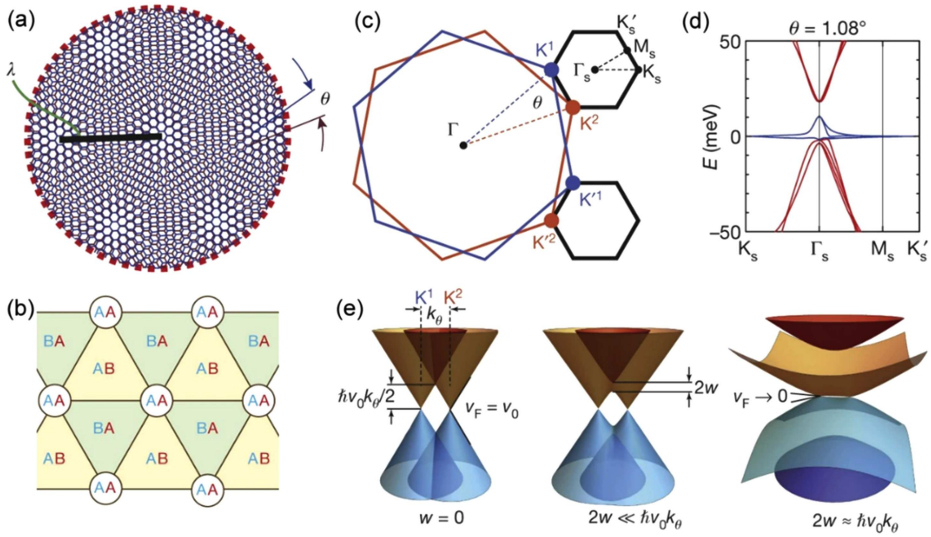


Fig. 2. Schematic representation of the TBG structure and electronic properties. (a) Illustration of the moiré pattern formed by the twisted bilayers. (b) Atomic configuration showing the AA, AB, and BA stacking regions. (c) Schematic image of the Brillouin zone of TBG with moiré mini Brillouin zone, where K'^1 and K'^2 correspond to the adjacent layers. (d) Electronic band structure at the magic angle ($\theta = 1.08^\circ$) showing the flat bands (Γ_s) and the transition points (K_s and K'_s), with the energy (E) measured in meV. (e) Intersection of the two Dirac cones changes with the interlayer hybridization w. Reproduced with permission from Ref. [1].

3. Orbital Magnetism in moiré superlattices of TBG

Graphene served as the inaugural model system for investigating nontrivial topological states, as first proposed by Haldane.[50] Subsequent advanced theoretical calculations have suggested that the QAH effect could be realized in graphene by incorporating exchange coupling and SOC.[51–53] However, little progress was made experimentally via this route due to the very weak SOC of graphene.

Surprisingly, the QAH effect was realized in TBG in combination with orbital magnetism. In TBG, moiré superlattices, in conjunction with interlayer coupling, induce band folding and the hybridization of Dirac cones within the mini-Brillouin zone. At the magic angle, strong interlayer coupling gives rise to two flat bands. These bands are positioned on either side of the Dirac point, with one serving as the conduction band and the other as the valence band. Each band exhibits a fourfold degeneracy across both spin and valley degrees of freedom. This degeneracy is symmetry-protected, ensuring its robustness against perturbations. Furthermore, the two valleys are characterized by Chern numbers of opposite signs. When the Fermi level lies within the flat bands, the moiré bands are partially filled, leading to symmetry breaking.[54] At this juncture, TRS is broken, and valley polarization potentially leads to orbital ferromagnetism.

Numerous calculations have demonstrated the presence of orbital magnetism and/or non-zero valley Chern numbers in magic-angle TBG.[55–62] Kang *et al.* reported that the interplay between Coulomb interactions and the kinetic energy of magic-angle TBG is crucial for understanding the correlated states. In the strong coupling regime, the Hamiltonian is simplified by considering only the interaction terms, with the kinetic energy treated as a perturbation.[63] This approach reveals that the effective Coulomb interaction, when projected onto the flat bands of TBG, can lead to symmetry-broken phases. For example, at $1/8$ filling, an insulating stripe $SU(4)$ ferromagnetic phase is possible, as shown in Figs. 3(a) and 3(b). Calculations by Xie *et al.* indicate that gapped states can form between the two flat bands at specific moiré band fillings

($p/4$, where $p < 4$ is an integer), as shown in Fig. 3(c).[64] Their theory suggests that at fillings of $\pm 1/4$ and $\pm 3/4$, these gapped states may break the valley-projected C_2T symmetry. The valleys exhibit the strongest possible polarization, which has significant implications for the occurrence of quantized AH effects.

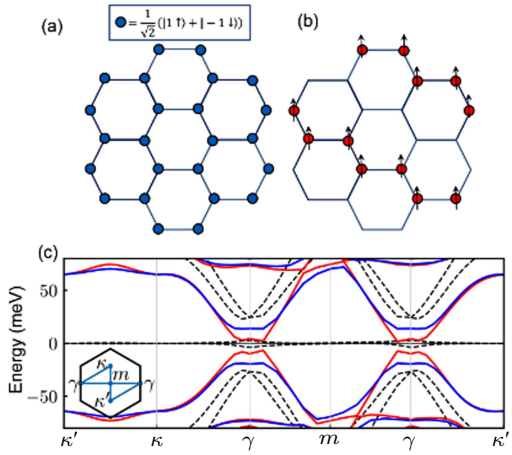


Fig. 3. Ferromagnetism in magic-angle TBG. (a) Mathematical representation of the $SU(4)$ ferromagnetic phase at $1/4$ filling, where spin nonmagnetism is present. (b) The stripe $SU(4)$ ferromagnetic insulator phase at $1/8$ filling. (c) Band structure of magic angle TBG at 1.1° and $\varepsilon = 5$. The band structure is shown in red where C_{2z} and TRS are preserved, and in blue where they are broken. The inset shows the moiré Brillouin zone and symmetry lines for the energy bands. (a) and (b) Reproduced with permission from Ref. [63]. (c) Reproduced with permission from Ref. [64].

4. AH effect in moiré superlattices of TBG

Although calculations have shown the potential for ferromagnetism and topologically nontrivial states in TBG induced by electron interactions, realizing the QAH effect remains challenging due to the difficulty in fabricating high-quality samples. The largest magic angle is approximately 1.08°, which is still difficult to achieve with high precision. TBG samples synthesized via chemical vapor deposition (CVD) and molecular beam epitaxy (MBE) typically exhibit fewer magic-angle grains,[32,65,66] a result of the structural instability at the relatively high total energy state characteristic of the magic-angle configuration. Currently, the fabrication of magic-angle TBG devices is most commonly accomplished through mechanical exfoliation using the "tear-and-stack" technique.[1,67–70] This method allows for the creation of TBG over large areas, with the specific size depending on the details of the fabrication process. However, this process is inevitably accompanied by bubbles and folds, which can lead to local strain, disorder, and trapped charges. Local strain introduces inhomogeneity of twist angle and can also affect the width of the flat bands.[42,43] Therefore, fabricating high-quality samples with homogeneous properties is essential for the emergence of strong correlations and the realization of the QAH effect.

In 2019, David *et al.* realized the AH effect near three-quarters filling ($3/4$) of the conduction miniband in magic-angle TBG devices with a twist angle of 1.2°. In TBG aligned with h-BN configurations, transport measurements revealed a hysteretic behavior in an applied out-of-plane magnetic field below 5 K, as shown in Figs. 4(a) and 4(b). The measurement of the transverse resistance (R_{xy}) exhibited significant AH resistance when the magnetic field was set to zero, indicating remanent magnetization, as shown in Fig. 4(a). The presence of a giant AH effect reflects the sample's magnetization, while a decrease in longitudinal resistance suggests the emergence of a Chern insulating phase. Furthermore, non-local transport measurements, including three-terminal and four-terminal resistances (Figs. 4(c) and 4(d)), provided evidence of chiral edge modes, which are characteristic signatures of a ferromagnetic topological insulator. Although some dissipation was observed, the potential for a giant AH resistance was demonstrated, supporting the possibility of a QAH effect in this system.

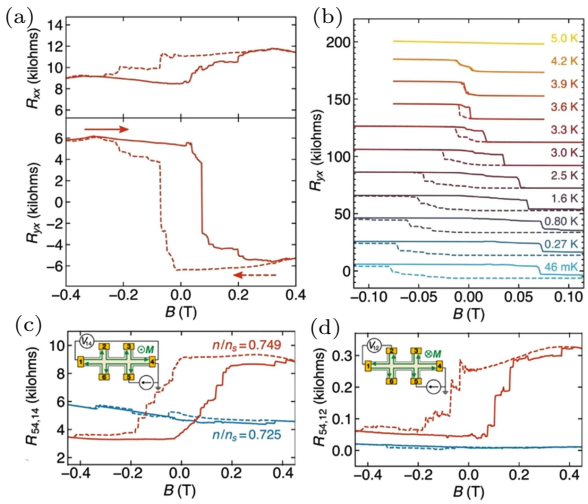


Fig. 4. Ferromagnetism and AH effect in TBG aligned with h-BN. (a) Plot of longitudinal resistance (upper panel) and Hall resistance (lower panel) as a function of magnetic field strength (B). (b) Hall resistance as a function of magnetic field strength (B) at various temperatures, indicated by the legend. The hysteresis loop diminishes as the temperature increases. Nonlocal transport measurements of three-terminal resistances (c) and four-terminal resistances (d). The inset images show diagrams of the corresponding experimental setups. Reproduced with permission from Ref. [5].

In theory, the realization of the QAH effect necessitates the formation of a Chern insulator state with a topologically nontrivial energy gap. As discussed in Section 2, lattice reconstruction effectively isolates the flat bands from higher energy bands. Moreover, the alignment of TBG devices with h-BN creates an energy gap between the conduction and valence bands, while assigning opposite Chern numbers to different valleys. At three-quarters filling of the conduction miniband in magic-angle TBG, TR symmetry, correlated with spin and valley degrees of freedom, undergoes spontaneous breaking. This phenomenon is pivotal to the realization of the QAH effect. Several theoretical frameworks have been proposed to elucidate the experimental findings.[71–73] For instance, Nick *et al.* employed the lowest Landau level model to highlight

the coupling between magic angle TBG and the encapsulating h-BN substrate. This configuration breaks the inherent 180° rotational symmetry (C_{2z}) of graphene, resulting in two Chern bands per valley. The two valleys carry opposite Chern numbers, with total Chern numbers $C = 0$, protected by TRS. When the TRS is broken by the spontaneous polarization of holes in spin and valley, induced by strong electron–electron interactions, the net Chern numbers $C \neq 0$, leading to the appearance of the AH state. Shortly thereafter, the AH effect was observed at more filling factors ($\nu = 1$ and ± 2),[74–76] even in TBG devices not aligned with h-BN.[74] In TBG without alignment with h-BN, strong electron interactions alone can also result in the nonzero Chern insulators at zero field.[74] Additionally, theoretical calculations have predicted the existence of both integer and fractional QAH effects in TBG aligned with h-BN.[71,72,77]

5. QAH effect in moiré superlattices of TBG

The transverse resistance of the QAH phase can be expressed as $R = h/(Ce^2)$, where h is Planck's constant, e is the electron's charge, and C is the Chern number, which arises from the integral of the Berry curvature over the energy bands. Further research on a more uniformly aligned magic-angle TBG/h-BN device with a twist angle of 1.15°, characterized by enhanced consistency in twist angle and charge distribution, successfully realized the QAH effect.[78] This work revealed a precisely quantized R_{xy} equivalent to h/e^2 with a Chern number $C = 1$ near the $3/4$ filling. Additionally, a suppression of the longitudinal resistance R_{xx} was observed even at $B = 0$ at this filling, confirming the existence of an integer quantum Hall insulator that integrates magnetism with nontrivial topological states, as shown in Figs. 5(a) and 5(b). In the single-particle band structure, each valley in graphene possesses bands with a finite Chern number; however, the overall Chern number for the entire system is zero. Strong correlations result in the spontaneous breaking of spin–valley symmetry, leading to an effective total Chern number of $C = 1$ and the emergence of orbital magnetism. Consequently, in contrast to magnetically doped TIs, electron interactions in flat-band systems play a crucial role in tuning both the topological states and magnetism — two essential ingredients in engineering the intrinsic QAH effect.

Additionally, temperature-dependent resistance measurements indicated that the quantized R_{xy} remains stable below 3 K, while the hysteresis persists up to 8 K, which aligns with the Curie temperature of 7.5 K associated with magnetic ordering, as shown in Fig. 5(c). These temperature-dependent behaviors are different from those observed in conventional systems of magnetically doped topological insulator films. The distinct characteristics of the QAH phase in flat-band systems suggest that electronic interactions play a key role in realizing the QAH effect at higher temperatures.

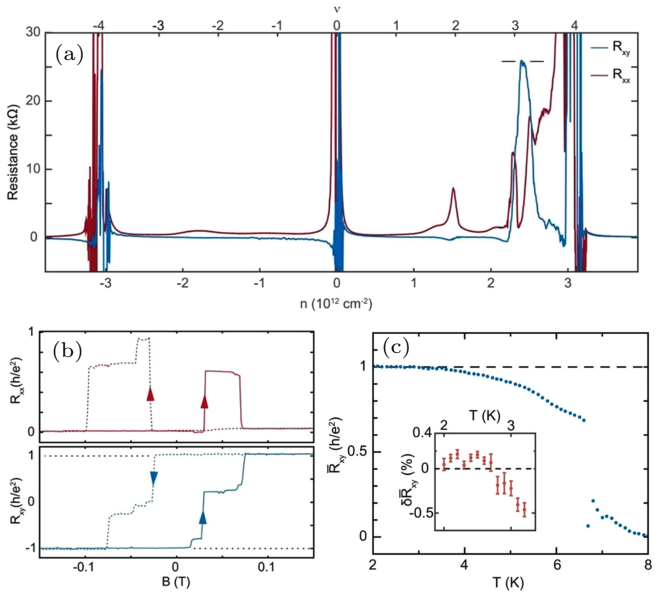


Fig. 5. QAH effect in TBG aligned with h-BN. (a) Longitudinal resistance R_{xx} (red) and Hall resistance R_{xy} (blue) as functions of carrier density n at a magnetic field of 150 mT. As the filling factor ν approaches 3, R_{xy} attains a quantized value of h/e^2 and R_{xx} approaches zero, signaling the emergence of a chiral edge state. (b) Dependence of both the longitudinal resistance and Hall resistance (R_{xy}) on the magnetic field, measured at $n = 2.37 \times 10^{12}$ cm^{-2} and $T = 1.6$ K. The Hall resistance R_{xy} shows hysteresis and maintains a quantized value of h/e^2 even at $B = 0$. (c) Field-training symmetrized Hall resistance $\bar{R}_{xy}$ as a function of temperature at zero magnetic field. $\bar{R}_{xy}$ remains quantized below 3 K. Reproduced with permission from Ref. [78].

6. FQAH effect in other moiré systems

The integer QAH states have been realized in magnetically doped TIs,[6] intrinsic magnetic TIs, such as $MnBi_2Te_4$,[7] and moiré superlattices including TBG/h-BN and heterobilayer TMDs.[82] However, the realization of FQAH effects remains a challenge due to the difficulty in identifying materials that exhibit both ferromagnetism and fractional Chern insulating behavior. Among the systems, fractional Chern insulator states have been successfully demonstrated in moiré superlattice configurations.[83,84] Moreover, although the moiré superlattice systems lack intrinsic magnetic properties in terms of their single-particle band structure, Coulomb interactions among electrons within the flat bands can lead to the emergence of ferromagnetic states and nontrivial topological features. Given the strong electronic correlations present in moiré systems, the realization of the FQAH effect in low-dimensional moiré materials is considered highly promising.

Xu *et al.* fabricated twisted moiré superlattices of bilayer $MoTe_2$ with a 3.7° twist angle and observed fractional Chern insulator characteristics in the absence of a magnetic field, indicative of the FQAH effect. These observations were made using photoluminescence and optical compressibility measurements, as shown in Figs. 6(a) and 6(b).[79] They as-

sessed the ferromagnetism and subsequently demonstrated the topological invariants of the ferromagnetic insulating states at fractional fillings. The reflective magnetic circular dichroism (RMCD) signal exhibited a non-zero intensity at zero magnetic field, along with a hysteretic response to the external magnetic field at fillings of $-1, -2/3$, and $-3/5$, suggesting the presence of ferromagnetism at these fillings. The photoluminescence intensity revealed linear dispersions with carrier density and magnetic field, particularly at the aforementioned fillings, persisting down to zero magnetic field. In accordance with the Středa formula, the Chern numbers of $-1, -2/3$, and $-3/5$ were extracted, and found to be consistent with both integer QAH and fractional QAH states. Although RMCD cannot directly provide the fractional quantized Hall conductance at zero magnetic field, it has demonstrated all the characteristics of the FQAH effect, including ferromagnetic states, topologically nontrivial states, and fractional insulating states at fractional filling factors $\nu = -2/3$ and $\nu = -3/5$.

The FQAH effect in twisted $MoTe_2$ was soon directly demonstrated by transport measurements.[80,85] For example, Xu *et al.* observed Hall resistances of h/e^2, $3h/e^2$ and $3h/(2e^2)$ with a Curie temperature of approximately 4 K, down to zero magnetic field in twisted $MoTe_2$ with a twist angle 3.7°, as shown in Fig. 6(c). The fractional Chern number, expected from the Streda formula, was $|C| = 0.6 \pm 0.05$, consistent with the anticipated $|C| = 2/3$. Meanwhile the local minimum of the longitudinal resistance indicated the emergence of chiral edge states. The applied vertical electric displacement field can tune the spontaneous TRS breaking and topologically trivial or nontrivial states. These evidences further demonstrate the robustness of the FQAH effect in the moiré superlattices of twisted $MoTe_2$.

Subsequently, the FQAH effect was also discovered in a graphene-based moiré system, specifically, rhombohedral pentalayer and hexalayer graphene/h-BN.[81,86,87] Additional fractional quantized Hall states were observed at filling factors of $\nu = 2/5, 3/7, 4/9, 4/7, 3/5, 2/3, 5/7, 3/4$ and $7/9$, attributable to the high material quality of the graphene-based moiré sample, as depicted in part of Figs. 6(d) and 6(e). The number of low-dimensional systems capable of exhibiting the QAH effect is rapidly increasing. In Table 1, we summarize these low-dimensional systems, including moiré and other flat-band systems. The checkmarks denote phases that have been successfully realized in experiments. Importantly, our summary may not include all possibilities due to the rapidly developing nature of this field.

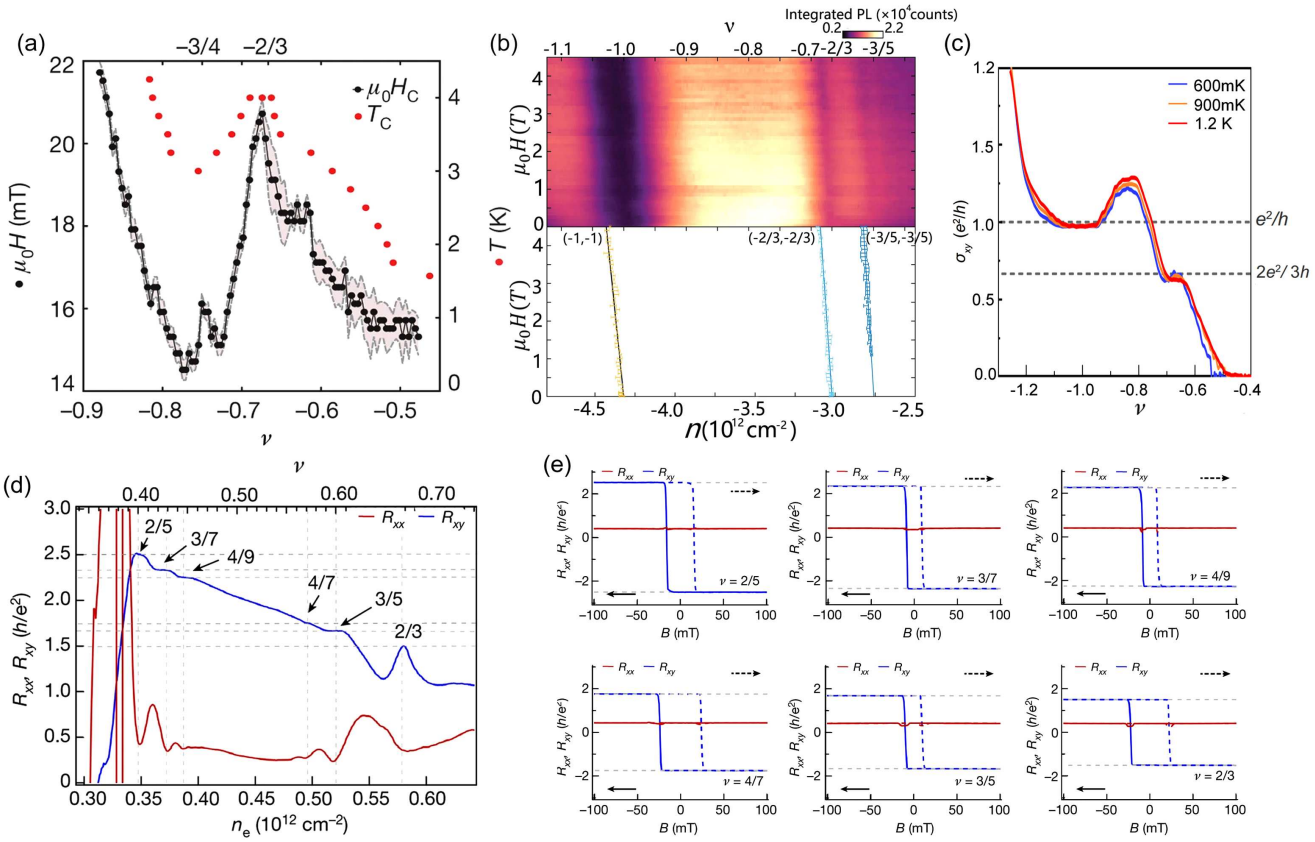


Fig. 6. FQAH effect in twisted $MoTe_2$ with twist angle 3.7° and graphene-based moiré system. (a) Coercive field $\mu_0 H$ and Curie temperature T_C as a function of filling factors ν. (b) Integrated PL intensity as a function of coercive field $\mu_0 H$ and carrier density n. (c) Hall conductivity σ_{xy} versus ν at 600 mK, 900 mK, and 1.2 K with the vertical electric displacement field $D = 5$ mV/nm. The obvious plateaus emerge near $\nu = -1$ and $-2/3$. (d) Longitudinal R_{xx} (red) and Hall resistances R_{xy} (blue) as functions of the carrier density n. Fractional Hall resistances emerge at filling factors ν of $2/5, 3/7, 4/9, 4/7, 3/5$ and $2/3$. (e) R_{xx} and R_{xy} show magnetic hysteresis at $\nu = 2/5, 3/7, 4/9, 4/7, 3/5$ and $2/3$. (a), (b) Reproduced with permission from Ref. [79]. (c) Reproduced with permission from Ref. [80]. (d), (e) Reproduced with permission from Ref. [81].

Table 1. An overview of the QAH related states realized in moiré and other 2D materials.

System(s)	AH effect	IQAH effect	FQAH effect	Refs.
Magic angle twisted bilayer graphene/h-BN	√	√	–	[3,5,74–76,78]
Twisted monolayer–bilayer graphene	√	√	–	[88–90]
ABC-trilayer graphene/h-BN	√	–	–	[91]
Bernal tetralayer graphene	√	–	–	[92]
Rhombohedral tetralayer graphene/h-BN	–	√	√	[87,93]
Rhombohedral pentalayer graphene/h-BN	–	√	√	[81,87,94]
Rhombohedral pentalayer graphene/WS_2 without moiré	–	√	–	[95]
Rhombohedral hexalayer graphene/h-BN	–	√	√	[86]
Twisted bilayer $MoTe_2$ (4°)	–	√	√	[79,80,85,96]
Twisted bilayer WSe_2	–	√	–	[97]
AB-stacked $MoTe_2$/WSe_2	–	√	–	[82]

7. Conclusion and perspectives

The QAH effect holds significant potential for practical applications, particularly in the realm of low energy devices, owing to its dissipationless chiral edge states. Recently, substantial progress has been made in realizing the QAH effect. In this review, we have discussed the evolution of the QAH effect in the prototypical moiré material, TBG aligned with h-BN. The structure and electronic properties of moiré materials can be significantly manipulated by adjusting the twist angles and interlayer coupling, resulting in a wide range of electronic behaviors. Notably, the long-range superlattices in these materials give rise to flat bands, which, in the case of magic-angle TBG, enable the realization of multiple correlated quantum phases due to strong electronic correlations. In TBG aligned with h-BN, the strong correlations, lattice reconstruction, and broken rotational symmetry facilitate the emergence of topologically nontrivial states and ferromagnetism. Furthermore, more exotic quantum phases, such as the FQAH effect, have been successfully realized in moiré materials. Table 1 summarizes the various exotic quantum states associated with QAH states in moiré and other flat-band systems. Notably, this table may not encompass all possibilities, as the rapidly evolving nature of the field may give rise to new theoretical insights.

Despite the significant progress in realizing the QAH phase in moiré materials, challenges remain for further advancements. First, there is a need for high-quality moiré samples.[98] Samples produced by mechanical exfoliation are often small and exhibit inhomogeneous twist angles, and suffer from strain. What's more, mechanically exfoliated samples have poor repeatability. More reliable methods, such as MBE or CVD, are needed to grow samples *in-situ*, with precise twist angles. Second, the temperature at which the QAH phase occurs is limited to a few Kelvins, which remains impractical for applications. The temperature at which the QAH effect is realized in magic-angle TBG aligned with h-BN coincides with the Curie temperature for magnetic ordering, presenting an opportunity to enhance this temperature through the optimization of moiré systems. Third, the potential emergence of Majorana zero modes within topological superconductors is an exciting avenue of research. This achievement could be realized at the interface between superconducting and QAH states.[99] Recent breakthrough by Choi *et al*. demonstrated the electrical tunability of both superconducting and QAH states in rhombohedral tetralayer graphene, highlighting the potential for such systems.[93] There is growing optimism that, in the near future, proximity effects could enable the realization of topological superconductors in low-dimensional moiré systems. Finally, the realization of FQAH effect provides us with an opportunity to investigate charge fractionalization, braiding (non-)Abelian anyons and topological quantum computation.

Thus far, the QAH phase has been realized in three systems: TIs with magnetic doping, $MnBi_2Te_4$ with intrinsic magnetism, and moiré materials with intrinsic magnetism. Uniquely, in moiré materials, the magnetism arises from orbital magnetism due to strong electronic correlations. The discovery of the QAH effect in TBG aligned with h-BN has opened new frontiers in the exploration of magnetic topological insulator phases driven by electronic correlations in moiré systems. Two-dimensional van der Waals materials provide an extensive materials platform for assembling moiré systems. In this context, there is a good possibility of identifying new materials that combine ferromagnetism with topological phases. These materials may realize the QAH and FQAH effects at elevated temperatures, bringing their application closer to realization.

Acknowledgements

This work was supported by the Science Research Project of Hebei Education Department (Grant No. BJK2024168), the National Natural Science Foundation of China (Grant No. 11904076), the Natural Science Foundation of Hebei (Grant No. A2019205313), and Science Foundation of Hebei Normal University (Grant No. L2024J02).

References

[1] Cao Y, Fatemi V, Demir A, Fang S, Tomarken S L, Luo J Y, Sanchez-Yamagishi J D, Watanabe K, Taniguchi T, Kaxiras E, Ashoori R C and Jarillo-Herrero P 2018 *Nature* **556** 80

[2] Cao Y, Fatemi V, Fang S, Watanabe K, Taniguchi T, Kaxiras E and Jarillo-Herrero P 2018 *Nature* **556** 43
[3] Lu X, Stepanov P, Yang W, Xie M, Aamir M A, Das I, Urgell C, Watanabe K, Taniguchi T, Zhang G, Bachtold A, MacDonald A H and Efetov D K 2019 *Nature* **574** 653
[4] Nuckolls K P, Oh M, Wong D, Lian B, Watanabe K, Taniguchi T, Bernevig B A and Yazdani A 2020 *Nature* **588** 610
[5] Sharpe A L, Fox E J, Barnard A W, Finney J, Watanabe K, Taniguchi T, Kastner M A and Goldhaber-Gordon D 2019 *Science* **365** 605
[6] Chang C Z, Zhang J, Feng X, Shen J, Zhang Z, Guo M, Li K, Ou Y, Wei P, Wang L L, Ji Z Q, Feng Y, Ji S, Chen X, Jia J F, Dai X, Fang Z, Zhang S C, He K, Wang Y, Lu L, Ma X C, Xue Q K 2013 *Science* **340** 167
[7] Deng Y, Yu Y, Shi M Z, Guo Z, Xu Z, Wang J, Chen X H and Zhang Y 2020 *Science* **367** 895
[8] Wu X C, Li S Z, Si J S, Huang B and Zhang W B 2024 *Chin. Phys. Lett.* **41** 057303
[9] Cui Q, Liang J, Zhu Y, Yao X and Yang H 2023 *Chin. Phys. Lett.* **40** 037502
[10] He K, Wang Y and Xue Q K 2014 *Natl. Sci. Rev.* **1** 38
[11] Grauer S, Schreyeck S, Winnerlein M, Brunner K, Gould C and Molenkamp L W 2015 *Phys. Rev. B* **92** 201304
[12] Chang C Z, Zhao W, Kim D Y, Zhang H, Assaf B A, Heiman D, Zhang S C, Liu C, Chan M H W and Moodera J S 2015 *Nat. Mater.* **14** 473
[13] Checkelsky J G, Yoshimi R, Tsukazaki A, Takahashi K S, Kozuka Y, Falson J, Kawasaki M and Tokura Y 2014 *Nat. Phys.* **10** 731
[14] Ou Y, Liu C, Jiang G, Feng Y, Zhao D, Wu W, Wang X X, Li W, Song C, Wang L L, Wang W, Wu W, Wang Y, He K, Ma X C and Xue Q K 2018 *Adv. Mater.* **30** 1703062
[15] Mogi M, Yoshimi R, Tsukazaki A, Yasuda K, Kozuka Y, Takahashi K S, Kawasaki M and Tokura Y 2015 *Appl. Phys. Lett.* **107** 182401
[16] Otrokov M M, Menshchikova T V, Vergniory M G, Rusinov I P, Vyazovskaya A Y, Koroteev Y M, Bihlmayer G, Ernst A, Echenique P M, Arnau A and Chulkov E V 2017 *2D Mater.* **4** 025082
[17] Li Q, Trang C X, Wu W, Hwang J, Cortie D, Medhekar N, Mo S K, Yang S A and Edmonds M T 2022 *Adv. Mater.* **34** 2107520
[18] Qi S, Gao R, Chang M, Han Y and Qiao Z 2020 *Phys. Rev. B* **101** 014423
[19] Sun K, Gu Z, Katsura H and Das Sarma S 2011 *Phys. Rev. Lett.* **106** 236803
[20] Zhang Y H, Mao D, Cao Y, Jarillo-Herrero P and Senthil T 2019 *Phys. Rev. B* **99** 075127
[21] Zhang Y, Tan Y W, Stormer H L and Kim P 2005 *Nature* **438** 201
[22] Bolotin K I, Ghahari F, Shulman M D, Stormer H L and Kim P 2009 *Nature* **462** 196
[23] Kane C L and Mele E J 2005 *Phys. Rev. Lett.* **95** 226801
[24] Novoselov K S, McCann E, Morozov S V, Fal'ko V I, Katsnelson M I, Zeitler U, Jiang D, Schedin F and Geim A K 2006 *Nat. Phys.* **2** 177
[25] Dean C R, Young A F, Cadden-Zimansky P, Wang L, Ren H, Watanabe K, Taniguchi T, Kim P, Hone J and Shepard K L 2011 *Nat. Phys.* **7** 693
[26] Li G, Luican A, Lopes Dos Santos J M B, Castro Neto A H, Reina A, Kong J and Andrei E Y 2010 *Nat. Phys.* **6** 109
[27] Tan L Z, Park C H and Louie S G 2011 *Nano Lett.* **11** 2596
[28] Yin L J, Qiao J B, Zuo W J, Li W T and He L 2015 *Phys. Rev. B* **92** 081406
[29] Li X F, Sun R X, Wang S Y, Li X, Liu Z B and Tian J G 2022 *Chin. Phys. Lett.* **39** 037301
[30] Zhao Y X, Zhou X F, Zhang Y and He L 2021 *Phys. Rev. Lett.* **127** 266801
[31] Brihuega I, Mallet P, González-Herrero H, Trambly De Laissardière G, Ugeda M M, Magaud L, Gómez-Rodríguez J M, Ynduráin F and Veuillen J Y 2012 *Phys. Rev. Lett.* **109** 196802
[32] Yan W, Liu M, Dou R F, Meng L, Feng L, Chu Z D, Zhang Y, Liu Z, Nie J C and He L 2012 *Phys. Rev. Lett.* **109** 126801
[33] Bistritzer R and MacDonald A H 2011 *Proc. Natl. Acad. Sci. USA* **108** 12233
[34] Guinea F and Walet N R 2018 *Proc. Natl. Acad. Sci. USA* **115** 13174
[35] Isobe H, Yuan N F Q and Fu L 2018 *Phys. Rev. X* **8** 041041
[36] Kennes D M, Lischner J and Karrasch C 2018 *Phys. Rev. B* **98** 241407
[37] Sherkunov Y and Betouras J J 2018 *Phys. Rev. B* **98** 205151
[38] Da Liao Y, Meng Z Y and Xu X Y 2019 *Phys. Rev. Lett.* **123** 157601
[39] Cea T and Guinea F 2020 *Phys. Rev. B* **102** 045107
[40] Kang J and Vafek O 2020 *Phys. Rev. B* **102** 035161
[41] Ren Y N, Zhang Y, Liu Y W and He L 2020 *Chin. Phys. B* **29** 117303
[42] Kazmierczak N P, Van Winkle M, Ophus C, Bustillo K C, Carr S, Brown H G, Ciston J, Taniguchi T, Watanabe K and Bediako D K 2021 *Nat. Mater.* **20** 956
[43] Huder L, Artaud A, Le Quang T, De Laissardière G T, Jansen A G M, Lapertot G, Chapelier C and Renard V T 2018 *Phys. Rev. Lett.* **120** 156405
[44] Yoo H, Engelke R, Carr S, Fang S, Zhang K, Cazeaux P, Sung S H, Hoyden R, Tsen A W, Taniguchi T, Watanabe K, Yi G C, Kim M, Luskin M, Tadmor E B, Kaxiras E and Kim P 2019 *Nat. Mater.* **18** 448
[45] Lucignano P, Alfè D, Cataudella V, Ninno D and Cantele G 2019 *Phys. Rev. B* **99** 195419
[46] Carr S, Fang S, Zhu Z and Kaxiras E 2019 *Phys. Rev. Res.* **1** 013001
[47] Zhou X F, Liu Y W, Hao C Y, Yan C, Zheng Q, Ren Y N, Zhao Y X, Watanabe K, Taniguchi T and He L 2023 *Phys. Rev. B* **107** 125410
[48] Gargiulo F and Yazyev O V 2018 *2D Mater.* **5** 015019
[49] Angeli M, Mandelli D, Valli A, Amaricci A, Capone M, Tosatti E and Fabrizio M 2018 *Phys. Rev. B* **98** 235137
[50] Haldane F D M 1988 *Phys. Rev. Lett.* **61** 2015
[51] Qiao Z, Yang S A, Feng W, Tse W K, Ding J, Yao Y, Wang J and Niu Q 2010 *Phys. Rev. B* **82** 161414
[52] Qiao Z, Ren W, Chen H, Bellaiche L, Zhang Z, MacDonald A H and Niu Q 2014 *Phys. Rev. Lett.* **112** 116404
[53] Tse W K, Qiao Z, Yao Y, MacDonald A H and Niu Q 2011 *Phys. Rev. B* **83** 155447
[54] Liu J, Ma Z, Gao J and Dai X 2019 *Phys. Rev. X* **9** 031021
[55] Zhang Y H, Mao D, Cao Y, Jarillo-Herrero P and Senthil T 2019 *Phys. Rev. B* **99** 075127
[56] Song J C W, Samutpraphoot P and Levitov L S 2015 *Proc. Natl. Acad. Sci. USA* **112** 10879
[57] Repellin C and Senthil T 2020 *Phys. Rev. Res.* **2** 023238
[58] Ochi M, Koshino M and Kuroki K 2018 *Phys. Rev. B* **98** 081102
[59] Dodaro J F, Kivelson S A, Schattner Y, Sun X Q and Wang C 2018 *Phys. Rev. B* **98** 075154
[60] Thomson A, Chatterjee S, Sachdev S and Scheurer M S 2018 *Phys. Rev. B* **98** 075109
[61] Venderbos J W F and Fernandes R M 2018 *Phys. Rev. B* **98** 245103
[62] Seo K, Kotov V N and Uchoa B 2019 *Phys. Rev. Lett.* **122** 246402
[63] Kang J and Vafek O 2019 *Phys. Rev. Lett.* **122** 246401
[64] Xie M and MacDonald A H 2020 *Phys. Rev. Lett.* **124** 097601
[65] Liu M, Zhang Y, Chen Y, Gao Y, Gao T, Ma D, Ji Q, Zhang Y, Li C and Liu Z 2012 *ACS Nano* **6** 10581
[66] Hass J, Varchon F, Millán-Otoya J E, Sprinkle M, Sharma N, De Heer W A, Berger C, First P N, Magaud L and Conrad E H 2008 *Phys. Rev. Lett.* **100** 125504
[67] Li S, Wang Z, Xue Y, Wang Y, Zhang S, Liu J, Zhu Z, Watanabe K, Taniguchi T, Gao H, Jiang Y and Mao J 2022 *Nat. Commun.* **13** 4225
[68] Guo H, Hu Z, Liu Z and Tian J 2021 *Adv. Funct. Mater.* **31** 2007810
[69] Purdie D G, Pugno N M, Taniguchi T, Watanabe K, Ferrari A C and Lombardo A 2018 *Nat. Commun.* **9** 5387
[70] Kim K, Yankowitz M, Fallahazad B, Kang S, Movva H C P, Huang S, Larentis S, Corbet C M, Taniguchi T, Watanabe K, Banerjee S K, LeRoy B J and Tutuc E 2016 *Nano Lett.* **16** 1989
[71] Bultinck N, Chatterjee S and Zaletel M P 2020 *Phys. Rev. Lett.* **124** 166601
[72] Repellin C and Senthil T 2020 *Phys. Rev. Res.* **2** 023238
[73] Zhang Y H, Mao D and Senthil T 2019 *Phys. Rev. Res.* **1** 033126
[74] Stepanov P, Xie M, Taniguchi T, Watanabe K, Lu X, MacDonald A H, Bernevig B A and Efetov D K 2021 *Phys. Rev. Lett.* **127** 197701
[75] Lin J X, Zhang Y H, Morissette E, Wang Z, Liu S, Rhodes D, Watanabe K, Taniguchi T, Hone J and Li J I A 2022 *Science* **375** 437
[76] Tseng C C, Ma X, Liu Z, Watanabe K, Taniguchi T, Chu J H and Yankowitz M 2022 *Nat. Phys.* **18** 1038
[77] Ledwith P J, Tarnopolsky G, Khalaf E and Vishwanath A 2020 *Phys. Rev. Res.* **2** 023237
[78] Serlin M, Tschirhart C L, Polshyn H, Zhang Y, Zhu J, Watanabe K, Taniguchi T, Balents L and Young A F 2020 *Science* **367** 900
[79] Cai J, Anderson E, Wang C, Zhang X, Liu X, Holtzmann W, Zhang Y, Fan F, Taniguchi T, Watanabe K, Ran Y, Cao T, Fu L, Xiao D, Yao W and Xu X 2023 *Nature* **622** 63

[80] Xu F, Sun Z, Jia T, Liu C, Xu C, Li C, Gu Y, Watanabe K, Taniguchi T, Tong B, Jia J, Shi Z, Jiang S, Zhang Y, Liu X and Li T 2023 *Phys. Rev. X* **13** 031037

[81] Lu Z, Han T, Yao Y, Reddy A P, Yang J, Seo J, Watanabe K, Taniguchi T, Fu L and Ju L 2024 *Nature* **626** 759

[82] Li T, Jiang S, Shen B, Zhang Y, Li L, Tao Z, Devakul T, Watanabe K, Taniguchi T, Fu L, Shan J and Mak K F 2021 *Nature* **600** 641

[83] Xie Y, Pierce A T, Park J M, Parker D E, Khalaf E, Ledwith P, Cao Y, Lee S H, Chen S, Forrester P R, Watanabe K, Taniguchi T, Vishwanath A, Jarillo-Herrero P and Yacoby A 2021 *Nature* **600** 439

[84] Spanton E M, Zibrov A A, Zhou H, Taniguchi T, Watanabe K, Zaletel M P and Young A F 2018 *Science* **360** 62

[85] Park H, Cai J, Anderson E, Zhang Y, Zhu J, Liu X, Wang C, Holtzmann W, Hu C, Liu Z, Taniguchi T, Watanabe K, Chu J H, Cao T, Fu L, Yao W, Chang C Z, Cobden D, Xiao D, Xu X 2023 *Nature* **622** 74

[86] Xie J, Huo Z, Lu X, Feng Z, Zhang Z, Wang W, Yang Q, Watanabe K, Taniguchi T, Liu K, Song Z, Xie X C, Liu J and Lu X 2024 arXiv: 2405.16944v1

[87] Lu Z, Han T, Yao Y, Yang J, Seo J, Shi L, Ye S,Watanabe K, Taniguchi T and Ju L 2024 arXiv: 2408.10203

[88] He M, Zhang Y H, Li Y, Fei Z, Watanabe K, Taniguchi T, Xu X and Yankowitz M 2021 *Nat. Commun.* **12** 4727

[89] Polshyn H, Zhu J, Kumar M A, Zhang Y, Yang F, Tschirhart C L, Serlin M, Watanabe K, Taniguchi T, MacDonald A H and Young A F 2020 *Nature* **588** 66

[90] Chen S, He M, Zhang Y H, Hsieh V, Fei Z, Watanabe K, Taniguchi T, Cobden D H, Xu X, Dean C R and Yankowitz M 2021 *Nat. Phys.* **17** 374

[91] Chen G, Sharpe A L, Fox E J, Zhang Y H, Wang S, Jiang L, Lyu B, Li H, Watanabe K, Taniguchi T, Shi Z, Senthil T, Goldhaber-Gordon D, Zhang Y and Wang F 2020 *Nature* **579** 56

[92] Chen H, Arora A, Song J C W and Loh K P 2023 *Nat. Commun.* **14** 7925

[93] Choi Y, Choi Y, Valentini M, Patterson C L, Holleis L F W, Sheekey O I, Stoyanov H, Cheng X, Taniguchi T, Watanabe K and Young A F 2024 arXiv: 2408.12584

[94] Aronson S H, Han T, Lu Z, Yao Y, Watanabe K, Taniguchi T, Ju L and Ashoori R C 2024 arXiv: 2408.11220

[95] Han T, Lu Z, Yao Y, Yang J, Seo J, Yoon C, Watanabe K, Taniguchi T, Fu L, Zhang F and Ju L 2024 *Science* **384** 647

[96] Zeng Y, Xia Z, Kang K, Zhu J, Knüppel P, Vaswani C, Watanabe K, Taniguchi T, Mak K F and Shan J 2023 *Nature* **622** 69

[97] Foutty B A, Kometter C R, Devakul T, Reddy A P, Watanabe K, Taniguchi T, Fu L and Feldman B E 2024 *Science* **384** 343

[98] Das Sarma S and Xie M 2024 *Phys. Rev. B* **109** L121104

[99] Qi X L, Hughes T L and Zhang S C 2010 *Phys. Rev. B* **82** 184516